THE JOURNAL OF PHYSICAL CHEMISTRY C
A JOURNAL OF THE AMERICAN CHEMICAL SOCIETY

pubs.acs.org/JPCC
Article

Reactivity of Organosilicon Additives with Water in Li-ion Batteries

Neeha Gogoi,* Wandi Wahyudi, Jonas Mindemark, Guiomar Hernández, Peter Broqvist, and Erik J. Berg*

Cite This: J. Phys. Chem. C 2024, 128, 1654−1662
Read Online

ACCESS | Metrics & More | Article Recommendations | Supporting Information

ABSTRACT: Introducing small volumes of organosilicon-containing additives as part of lithium-ion battery (LIB) electrolyte engineering has been getting a lot of attention owing to these additives' multifunctional properties. Tris(trimethylsilyl)phosphate (TMSPa) is a prominent member of this class of additives and scavenges Lewis bases such as water, although the rate at which the reaction occurs and the fate of the resultant product in the battery system still remain unknown. Herein, we have employed complementary nuclear magnetic resonance and gas chromatography−mass spectrometry to systematically study the reactivity of TMSPa with water in conventional organic carbonate solvents mimicking the Li-ion cell environment. The reaction products are identified, and a working reaction pathway is proposed by following the chemical evolution of the products over varying time and temperatures. We found that the main reaction products are trimethylsilanol (TMSOH) and phosphoric acid (H_3PO_4); however, various P−O−Si-containing intermediates were also found. Similar to water, the Lewis base TMSOH can undergo reaction with TMSPa at room temperature to form hexamethyldisiloxane and can also activate ethylene carbonate (EC) ring-opening reactions at elevated temperatures (≥80 °C), yielding a TMS derivative with ethylene glycol (TMS-EG). While the formation of TMS-EG at the expense of EC is in principle an unwanted parasitic reaction, it should be noted that this reaction is only activated at elevated temperatures in comparison to EC ring-opening by H_2O, which takes place at ≥40 °C. Thus, the study underlines the advantages of organo-silicon compounds as electrolyte additives. Elucidating the reaction mechanism in model systems like this is important for future studies of similar additives in order to improve the accuracy of additive exploration in LIBs.

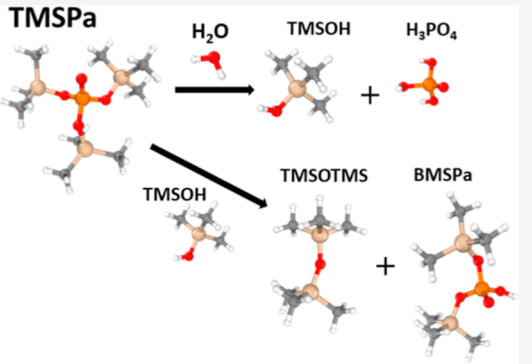

INTRODUCTION

The electrolyte plays a crucial role in lithium-ion batteries (LIBs) by providing Li^+ transport between the positive and negative electrodes during the charge and discharge. The electrolyte also has to guarantee the formation of chemically stable electrode passivation layers [such as the solid−electrolyte interphase (SEI) on graphite anodes] since the electrodes operate already at or beyond its thermodynamic stability. State-of-the-art electrolytes in commercial LIBs are nonaqueous and based on lithium hexafluorophosphate ($LiPF_6$) salt dissolved in organic carbonate solvent mixtures. The strict incompatibility of these electrolytes toward moisture is however a challenge. All electrolyte components are sensitive toward hydrolysis, which in turn further triggers electrolyte degradation and accelerated battery decay.[1]

Electrolyte engineering by the introduction of additives (typically up to 5% per volume or weight) is a viable strategy to enhance the performance of the electrolyte and the battery. Recently, additive molecules containing organosilicon groups have been receiving a lot of recognition owing to their multifunctional properties. In a comparative study, Dahn and co-workers identified that an organosilicon-derived trivalent phosphorus(III)-based additive [tris(trimethylsilyl)phosphite, hereafter denoted as TMSPi] provides improved Li-ion cell properties when added along with vinylene carbonate (VC) in $LiNi_{1/3}Mn_{1/3}Co_{1/3}O_2$ (NMC111)/graphite pouch cells.[2] The cell containing TMSPi exhibited longer cycle life, longer calendar life, and reduced impedance compared to those of a cell with VC alone, which they attribute to a slower rate of parasitic side reactions in the presence of the TMSPi. Han et al. have also proposed that TMSPi serves as an effective scavenger of detrimental HF that is generated near the cathode surface. TMSPi consumes acidic HF, preventing the corrosion of the cathode by rather forming organophosphoric acid and organofluorine-based compounds.[3] The products thus formed positively affect the cathode/electrolyte interface. A study by Abraham and group further concluded that incorporation of TMSPi in NMC532/graphite cells facilitates the formation of a beneficial positive electrode surface film lowering the capacity

Received: November 14, 2023
Revised: December 21, 2023
Accepted: January 2, 2024
Published: January 23, 2024

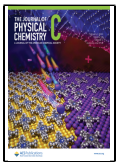

fade of the cell.[4] Upon X-ray photoelectron spectroscopy analysis, they found that the surface deposits are rich in P- and O-containing species and postulated that the scission of the trimethylsilyl (TMS) groups from TMSPi helps the central phosphite moiety of the reactive additive molecule intermediate bind to oxygen atoms at the oxide surface and form a protective surface film. On the other hand, Liao et al. detected Si-containing residues from TMSPi on the surface of the lithium nickel cobalt manganese oxide cathode after cycling. They claimed that these are formed as oxidative decomposition products, which can suppress further electrolyte decomposition on the cathode surface.[5]

Another additive molecule belonging to the same family of silyl-ester-based additives is tris(trimethylsilyl)phosphate (TMSPa), which connects three organosilicon groups (TMS) to a central phosphate. It has been shown that TMSPa exhibits the same beneficial effect as TMSPi and that the phosphate compound acts in a more subtle way compared to TMSPi.[6,7] Bolli et al. showed that TMSPa, and molecules alike such as TMSPi, scavenges not only HF but also fluorides (e.g., LiF) formed during the operation of the Li-ion cells. The results, however, concluded that electrode surface layers [SEI or cathode−electrolyte interphase (CEI)] largely remain unaffected by the presence of TMSPa during the initial formation cycles of the cell.[8] Our recent study reported that the reactivity of TMSPa is not only limited to fluorides, but it could be extended to other Lewis bases (LBs) generated/present in LIBs, such as water, hydroxides, and alkoxides.[9] These LBs are generally harmful since they decompose the organic carbonate solvents, yielding CO_2 and glycols. By including small amounts of TMSPa in the electrolyte, such adverse effects can be mitigated by simply removing the LBs. The molecular mechanism behind the scavenging of LBs relies primarily on the Si−O bond of the TMSPa undergoing cleavage while reacting with the LBs forming presumably less harmful organosilicon residues (TMS-LB) as products. For instance, we recently showed that TMSPa scavenges H_2O, in an environment of ethylene carbonate (EC)/ diethyl carbonate (DEC) mixture (1:1 v/v), forming TMSOH. Calculations of the first step of the TMSPa/H_2O reaction showed that the hydrolysis of TMSPa is slightly exothermic. However, the later steps in the H_2O and TMSPa reaction mechanism were not clarified. H_2O is an unavoidable impurity present in organic electrolytes and is well-known to detrimentally affect all components of the battery. Reduction of H_2O leads to evolution of H_2 and LiOH formation, whereby the latter ring-opens the cyclic carbonate solvent, such as EC, as mentioned above.[9] Despite numerous reports on the observation of Si−O bond cleavage and the formation of different silane-derived species in batteries containing TMSPa, a complete understanding of the underlying reaction pathways is lacking.

The aim of the study is to determine the reaction mechanism of TMSPa with H_2O residues in organic carbonate solvents commonly used in Li-ion batteries. Our hypothesis is that TMSPa scavenges H_2O to form less harmful silyl-group-containing compounds other than TMSOH as previously postulated. The reaction mechanism of TMSPa is investigated via nuclear magnetic resonance (NMR) and gas chromatography−mass spectrometry (GC−MS) as well as molecular dynamics coupled with density functional theory (MD−DFT).

METHODS

Preparation of the Sample Solutions. Battery-grade EC (Sigma-Aldrich) and DEC (Sigma-Aldrich) were introduced into an Ar closed glovebox (O_2, H_2O content <1 ppm) as received from the suppliers. DEC was dried with molecular sieves and then mixed with EC (which was heated up to 45 °C to melt). The mixture of EC/DEC used in this study is in a 1:1 volume ratio, unless otherwise stated. The EC/DEC was deliberately contaminated with 2 vol % H_2O, and then, the mixture was stored at room temperature (RT) while being magnetically stirred for 24 h. Then, the sample was left for at least 12 h for it to equilibrate. Then 5 vol % TMSPa from Sigma-Aldrich was added into the mixture. 1,1,1,3,3,3-Hexamethyldisiloxane (TMSOTMS) and trimethylsilanol (TMSOH) from Sigma-Aldrich were used as-received from suppliers. After the reaction, the solution was extracted for visual inspection and qualitative assessment of the resulting compounds under NMR.

Nuclear Magnetic Resonance. For NMR, a JEOL (^{1}H, 400 MHz; ^{31}P, 162 MHz; ^{29}Si, 376 MHz) spectrometer (JEOL ECZ 400S) was used, and chemical shifts were recorded in parts per million. Fluorinated ethylene propylene (FEP) NMR tube liners (outer diameter: 5 mm, Wilmad-LabGlass) with anhydrous dimethyl sulfoxide (DMSO)-d_6 (99.9%) from VWR was used as the deuterated solvent. The mouth of the FEP tube was closed with a poly(tetrafluoroethylene) (PTFE) plug. Each FEP NMR tube containing 300 μL of DMSO-d_6 was placed inside a glass NMR tube (inner diameter: 5 mm) containing 150 μL of the sample solution. The glass tube was again closed with a PTFE stopper. Any interaction between the deuterated solvent and reaction mixtures that could result in an undesirable reaction was strictly prohibited. The solution storage and sample preparation were done in the glovebox, and the H_2O content inside it was kept below 1 ppm. All spectra were processed and analyzed with MestReNova 6.0.2−5475. The ^{1}H and ^{13}C NMR signals were internally referenced to the signal of DMSO-d_6 at 2.46 and 39.6 ppm, respectively.

Temperature variation in the mixture from RT to 80 °C (steps every 10 °C) in the NMR tube was performed to accelerate the chemical reactions. The mixture was held at each stated temperature for 8 h before recording the spectra. During the spectrum recording, the temperature was brought back to RT to not have any effect on the overall chemical shifts of the NMR signals.

A few of the selected samples were then extracted and analyzed with GC−MS.

Gas Chromatography−Mass Spectrometry. The experiments with liquid injections were done with an injection volume of 0.1 μL. The GC−MS measurements were done with a Shimadzu GC−MS QP2020 NX W/O RP 230 V equipped with an AOC-20i Plus stand-alone auto injector. A GC capillary (SH-200MS; 0.25 mm ID; 1.00 μm df; 30 m) column was used. The system was controlled by the GC−MS real-time analysis, and the chromatograms were analyzed with GC−MS postrun analysis (both from Shimadzu). Compounds were validated with the NIST 11 library. Helium (99.999% purity, Alphagaz) was used as carrier gas with a 1.16 mL min^{-1} column flow and 3 mL min^{-1} purge flow. The temperature program started at 100 °C which was held for 1 min. The temperature was ramped at 30 °C min^{-1} until 280 °C and held at 280 °C for 1 min. The overall measurement time was 11 min with a mass range from 25 to 700 m/z and an event time of 0.1

https://doi.org/10.1021/acs.jpcc.3c07505
J. Phys. Chem. C 2024, 128, 1654−1662

s in scan mode. The mass spectrometer was run in the electron impact ionization mode with the following parameters: the temperature of the ion source was set to 220 °C; the interface was held at 250 °C, and the filament was operated at a voltage of 70 V; and the detector voltage was set relative to the respective tuning results. The values presented in this work are reported as relative intensity with respect to the highest peak in the specific measurement, i.e., the DEC peak.

Computational Method. Electronic structure calculations based on van der Waals (vdW)-corrected hybrid DFT was performed for gas-phase reactions of TMSPa with LBs in a previous study.[9] Besides the actual scientific results, those computations demonstrated the importance of including solvation effects in order to find a correlation between the computational and experimental observations. It was found that the electrostatic interaction between the solvated molecules was very different, leading to larger lowering for the reaction products, and thereby lowering the reaction free energy. To ensure that such effects are accounted for in this work, we devised a computational protocol based on a combination of static hybrid-DFT calculations and machine learning (ML)-accelerated long-time-scale molecular dynamics simulations (MD) of solvated reactants and products. In this protocol, 0 K reaction energies, i.e., the breaking and formation of intramolecular chemical bonds, are calculated at the hybrid DFT level of theory using Gaussian09.[10] More specifically, we use the B3LYP functional,[11−14] the local aug-cc-pVDZ basis set for the expansion of the electron wave functions. Weak nonlocal interactions (vdW forces) were accounted for using the Grimme D3 vdW correction scheme.[15] All structures were geometrically optimized until the forces on each atom were less than 0.00077 eV/Å. The computed reaction energies were further corrected using relative solvation energies obtained from ML-accelerated MD simulations of solvated reactants and products using the PiNN ML model[16] trained on data computed using the GFN2-xTB semiempirical model by Grimme et al.[17,18] The GFN2-xTB model is generally good at describing geometries and intermolecular bond energies of molecular systems. The ML-accelerated MD simulations rely on an adaptive learning-on-the-fly workflow developed by Shao et al.[19] The PiNN model relies on PiNet, which is a high-performance graph convolutional neural network. The PiNN model was trained for 5 elements (H, C, O, Si, and P). The model has been trained so that the error with respect to the reference calculations in the reported data is smaller than 0.02 and 2.00 eV/Å for energies and forces, respectively.

The MD simulations with the PiNN model were performed within the *NPT* ensemble using a Berendsen thermostat at 340 K as implemented in the ASE ecosystem.[20] In total, 40 different MD simulations were performed for various combinations of reactants and products solvated in EC for the training. The initial configurations were obtained using PackMoL[21] with the solvated molecule embedded in 15 EC molecules in a box with periodic boundary conditions. After the training, additional production runs were performed for the reactants and products of a total of 512 ps using the same box sizes. The time step used in the simulations was 1 fs in order to account for the movement of the light hydrogen atoms. The resulting relative solvation energies were averaging total energies from the last 200 ps for each solvated species.

RESULTS AND DISCUSSION

Identifying the Reaction Pathways of TMSPa with H_2O. Figure 1a, b and c presents the ^{31}P NMR spectra of 5 vol % TMSPa dissolved in the EC/DEC mixture that is contaminated with three different concentrations of H_2O, i.e., 0.5, 2, and 5 vol %, respectively. The ^{31}P spectrum for the solution containing 0.5v % H_2O (Figure 1a) shows a strong signal at −24.60 ppm corresponding to TMSPa. The weak signal at −13.90 ppm is identified as BMSPa (bis-(trimethylsilyl)phosphate), which represents TMSPa that has lost one TMS unit, formed from reaction 1.

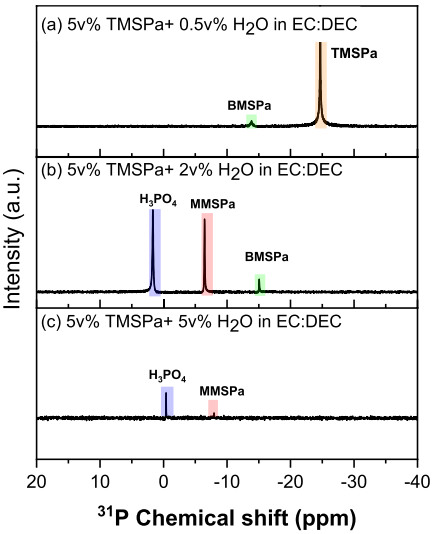

Figure 1. ^{31}P NMR of 5 vol % TMSPa added in EC/DEC that is contaminated with (a) 0.5, (b) 2, and (c) 5 vol % H_2O in the EC/DEC. TMSPa chemically reacts with H_2O in a carbonate-based solvent system to form BMSPa, MMSPa, and H_3PO_4.

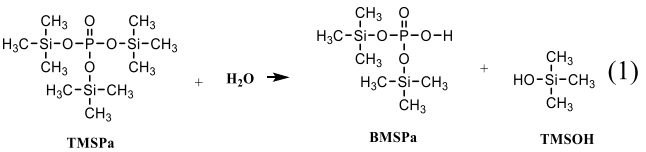

(1)

The presence of a strong TMSPa signal indicates that there is a significant amount of unreacted TMSPa left in the solution. The spectrum for the solution containing 2 vol % H_2O (Figure 1b) shows the existence of three signals at −15.16, −6.36, and 1.95 ppm. The signal at −15.16 ppm is again identified as BMSPa, while the signal at −6.36 ppm corresponds to mono(trimethylsilyl)phosphate (MMSPa), which represents TMSPa that lost two TMS units), e.g., as formed from reaction 2.

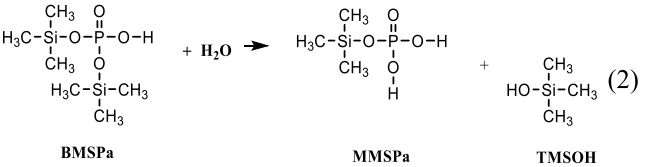

(2)

There are no peaks corresponding to TMSPa, indicating that TMSPa was mostly consumed during the chemical reactions. The compound exhibiting the strong signal at −0.33 ppm is

https://doi.org/10.1021/acs.jpcc.3c07505
J. Phys. Chem. C 2024, 128, 1654−1662

identified as phosphoric acid (H_3PO_4), e.g., as formed from chemical reaction 3.

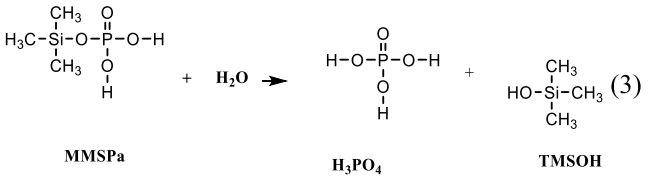

(3)

Finally, the spectrum for the solution containing 5 vol % H_2O (Figure 1c) shows two signals, one at −0.33 ppm and another very weak signal at −8.00. These two signals are assigned to H_3PO_4 and MMSPa, respectively. These chemical shifts are in close agreement to those reported in our previous paper, where we have observed these intermediates formed during the reaction between LiOH and TMSPa in carbonate solvent mixtures.[9]

It is also to be noted that chemical shifts are influenced by the concentrations, solvation structures, and hydrogen bonding of the chemical species, which could explain the slight variations in the chemical shifts of the species. H_3PO_4 is the proposed end product of the reaction between TMSPa and H_2O when all TMS units left in the TMSPa molecule. The highly electrophilic TMS group likely acts as an anion receptor, accepting OH^- and forming TMSOH. Therefore, in a practical Li-ion cell, TMSPa is expected to scavenge H_2O and therefore eliminate the undesired side reactions triggered by H_2O, discussed above. TMSOH, formed as a side product, is identified by ^{29}Si NMR, and it will be discussed in the later part of this section.

^{1}H NMR spectra for TMSPa and H_2O mixtures in the EC/DEC are shown in figure S1 in the Supporting Information (DMSO-d_6, 25 °C). The TMSPa methyl protons give rise to a singlet at −0.02 ppm. Due to the similar structure of TMSPa and BMSPa (/MMSPa), the methyl protons appear close to each other at −0.02 ppm and the −OH resonance appears at 5.09 ppm (Supporting Information Figure S1). TMSPa readily establishes an equilibrium with TMSOH and BMSPa (/MMSPa) in solution in the presence of 2 vol % H_2O. Increasing the amount of H_2O, while keeping the amount of TMSPa constant in the reaction mixture (5 vol % TMSPa in EC/DEC contaminated with 5 vol % H_2O), forces the equilibrium of reaction 1 to further right, favoring the formation of TMSPa molecule, which has lost at least one of its TMS units and hence TMSOH. On the other hand, lowering the amount of H_2O in the mixture (5 vol % TMSPa in EC/DEC contaminated with 1 vol % H_2O) shows that the reaction stops at BMSPa, while most of TMSPa remains unreacted in the solution.

The effect of the temperature on the chemical reactions was investigated in-situ by ramping the temperature during the NMR experiments up to 80 °C, with the aim to accelerate the chemical reactions. The sample with 2 vol % H_2O in EC/DEC with 5 vol % TMSPa added was heated to 80 °C, and NMR spectra were recorded in-situ to track the evolution of the stable reaction products. No change in the signal of TMSPa, BMSPa, and MMSPa was observed in the ^{31}P NMR spectra (as presented in Figure S2), except for a slight broadening of all of the signals. In order to further confirm the proposed reaction products (TMSOH, BMSPa, and MMSPa), ^{29}Si NMR spectra of the mixture at varying temperatures (from 30 to 80 °C) were analyzed. The spectra for the sample recorded at RT after heating to 30 and 80 °C are presented in Figure 2a,b, respectively (^{29}Si NMR spectra of the mixtures in the intermediate temperature steps can be found in the Supporting Information, figure S3).

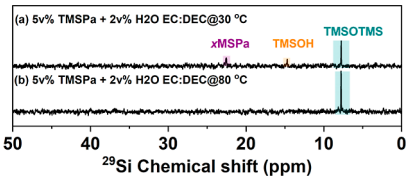

Figure 2. ^{29}Si NMR of 2 vol % H_2O in EC/DEC with 5 vol % TMSPa at (a) 30 and (b) 80 °C.

The signal at ∼15 ppm in the ^{29}Si NMR spectrum (Figure 2) observed in the sample at 30 °C is attributed to TMSOH. The reaction intermediates BMSPa and MMSPa however cannot be differentiated from the TMSPa signal observed at ∼25 ppm in the ^{29}Si spectrum of the sample (represented as *x*MSPa). It is assumed that these products (TMSPa, BMSPa, and MMSPa) have very similar chemical shifts and, due to the low sensitivity of the ^{29}Si NMR, could not be distinguished in the ^{29}Si spectra. Interestingly, the strongest peak at ∼7 ppm observed for the mixtures is assigned to TMSOTMS. These results point toward an alternative reaction pathway between TMSPa and H_2O, where TMSOTMS is one of the most stable end products. One way to explain this is that the eliminated reaction product TMSOH (formed from reactions 1−3) further dimerizes to give TMSOTMS and water (reaction 4).

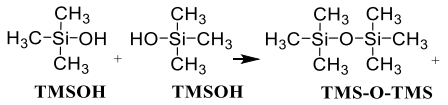

(4)

If this is the case, then H_2O is regenerated, which, in turn, could hypothetically again react with TMSPa. Another possibility is that if instead of H_2O (OH^-) attacking the additive molecule further on, the TMSOH formed during the reaction attacks TMSPa in a subsequent step with its TMSO-unit, breaking TMSPa's O−Si bond. In this case, TMSOTMS is the most likely reaction product along with BMSPa (reaction 5).

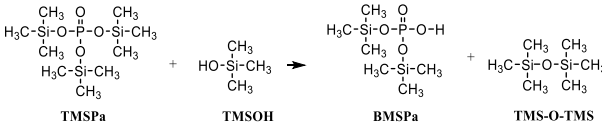

(5)

In order to confirm which reaction dominates, 5 vol % TMSPa was added to an EC/DEC mixture containing 2 vol % TMSOH. The ^{29}Si NMR spectrum presented in Figure 3 indeed confirms the formation of TMSOTMS. However, TMSPa and TMSOH could not be detected in the spectrum, which indicates that TMSPa and the TMSOH have been consumed in the chemical reaction. The corresponding ^{31}P NMR spectrum (in Figure 3 inset) of the sample mixture shows the formation of BMSPa. A very weak signal for residual TMSPa is detected in the ^{31}P NMR spectrum.

Thus, this experiment confirms that TMSOTMS and BMSPa are formed due to the reaction of TMSPa and TMSOH and, furthermore, the TMSO-group of the excess TMSOH molecules could attack the BMSPa in the following

https://doi.org/10.1021/acs.jpcc.3c07505
J. Phys. Chem. C 2024, 128, 1654−1662

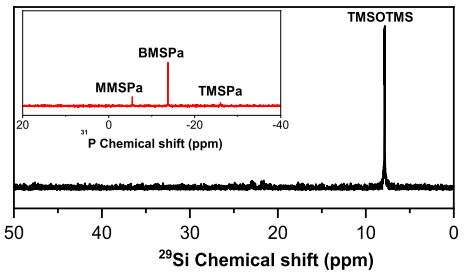

Figure 3. ^{29}Si NMR spectrum of 5 vol % TMSPa added to EC/DEC containing 2 vol % TMSOH sample mixture. The inset shows the corresponding ^{31}P NMR spectrum.

reaction step, resulting in the formation of TMSOTMS and MMSPa as final products (reaction 6).

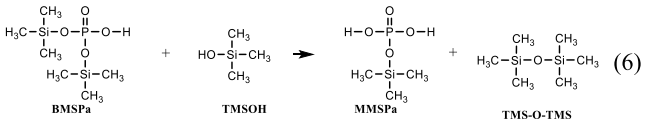

(6)

These findings explain the presence of a signal of MMSPa in the ^{31}P NMR spectrum, as seen in the inset of Figure 3. Indeed, Yim et al. and Winter et al. showed the formation of TMSOTMS due to the *O*-silylation of TMSPi triggered by TMSOH.[3,22,23] The fact that the signal for TMSOTMS in the TMSPa-added EC/DEC mixture containing 2 vol % H_2O grows as the temperature increases in the ^{29}Si NMR spectrum as seen in Figure 2 while that for TMSOH and TMSPa disappears indicates that the reaction of TMSOH with TMSPa forming TMSOTMS is further enhanced at elevated temperature.

Interestingly, TMSOTMS is also detected in trace amounts in pure TMSPa and TMSOH according to NMR analysis (Figure S3). The peak at ∼7 ppm in ^{29}Si NMR spectra denotes the presence of TMSOTMS. Thus, based on spectroscopic evidence, it can be said that TMSPa is very sensitive toward impurities, even if those impurities are present in very low amounts. The Si−O bond of TMSPa undergoes cleavage owing to the high affinity of Si toward nucleophiles (O−, OH−, F−, and OCH_3−). This would eventually result in the TMSOTMS and BMSPa. BMSPa was indeed observed in the ^{31}P NMR spectrum for the pure TMSPa (figure S4).

In a first attempt, in our simulations of hydrolysis of TMSPa forming BMSPa, MMSPa, H_3PO_4, TMSOTMS, and TMSOH according to reactions 1−8, we used gas phase molecules to compute the energy of reaction.

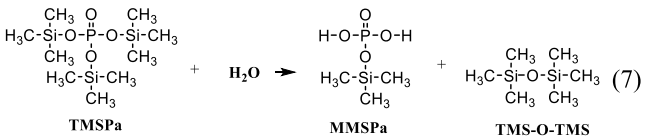

(7)

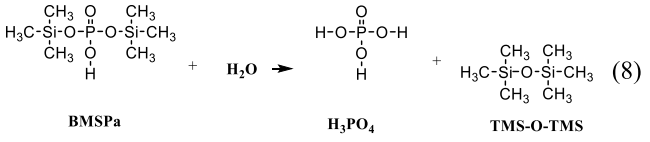

(8)

Reactions 7 and 8 are basically the direct chemical reaction steps that take into account the formation and subsequent reaction of BMSPa (/MMSPa) with TMSOH leading to MMSPa (/H_3PO_4) and dimer formation. These reactions are represented as red lines in the energy diagram in Figure 4.

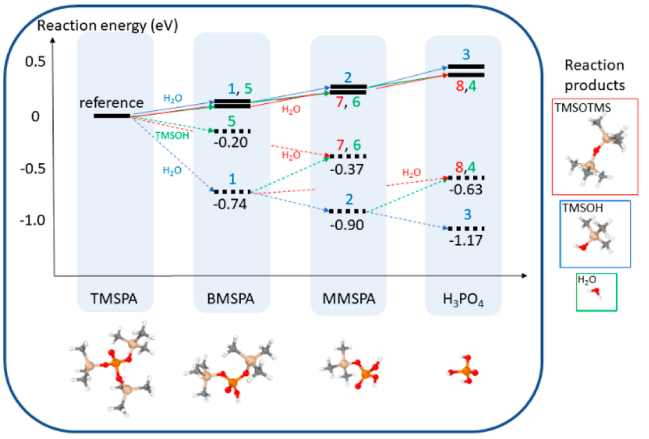

Figure 4. Reaction energy diagram with energies in eV for the TMSPa decomposition to H_3PO_4 using water as reagent. The reactions are numbered sequentially as they appear in the paper. In addition to reactions 1−6, two more chemical reactions are computed in the energy diagram (reaction 7 and 8, as described in the paragraph below). The solid lines are used to denote the reaction energies computed using noninteracting reactants and products (gas phase). The dashed lines are used to denote the energies computed involving an explicit EC solvent molecule to ensure that all hydrogen bonds are accounted for (see the Computational Method section for details). The inset shows the molecular structure of TMSPa, BMSPa, MMSPa, H_3PO_4, TMSOTMS, TMSOH, and H_2O. The orange ball is P, beige balls are Si, gray balls are C, red balls are O, and white balls are H.

Interestingly, the energy of reaction ΔE was always found to be endothermic ($\Delta E > 0$). The lowest ΔE for the various reactions is schematically illustrated in Figure 4 (assigned with solid lines). However, if we allow for intermolecular interactions between the reactants and the products with the electrolyte solvent, here explicitly treated through our scheme described in the computational section, the ΔE for the reactions becomes negative, which implies that the reactions are exothermic and spontaneous (as can be seen in Figure 4, denoted with dashed lines). Thus, in order to obtain theoretical results that correlate with the experimental observations, it is important to account for explicit noncovalent interactions to stabilize the product side. The reason for this is the increased electrostatic interaction between the EC and OH groups on the remaining BMSPa and TMSOH compared to the methyl-EC and water-EC interaction on the reactant side. From the simulations, we conclude that TMSPa spontaneously reacts with H_2O to form BMSPa. The computations furthermore suggest that the reactions that lead to the formation of MMSPa and H_3PO_4 in the subsequent step (reactions 2 and 3) are less energetically favorable compared to the first step (reaction 1).

Furthermore, the computed reaction energies show that the reactions between TMSPa (/BMSPa) and TMSOH forming TMSOTMS (reactions 5 and 6) are slightly exothermic, which matches the experimental observations reported earlier. These results suggest that the ability of the reaction product to form energetically favorable intermolecular interactions (primarily hydrogen bonding) is important for an efficient breakage of the O−Si bond of TMSPa.

https://doi.org/10.1021/acs.jpcc.3c07505
J. Phys. Chem. C 2024, 128, 1654−1662

Identifying the Stability of TMSOH in EC/DEC. Having established that TMSOH is a rather reactive intermediate during the hydrolysis of TMSPa, we further elucidate an alternative fate of the compound, which potentially affects practical cell performance. For that purpose, 5 vol % TMSOH was introduced in EC/DEC and then analyzed using NMR spectroscopy. The ^{13}C, ^{1}H, and ^{29}Si NMR spectra of the mixture are shown in Figure 5a(i),b(i), and c(i), respectively.

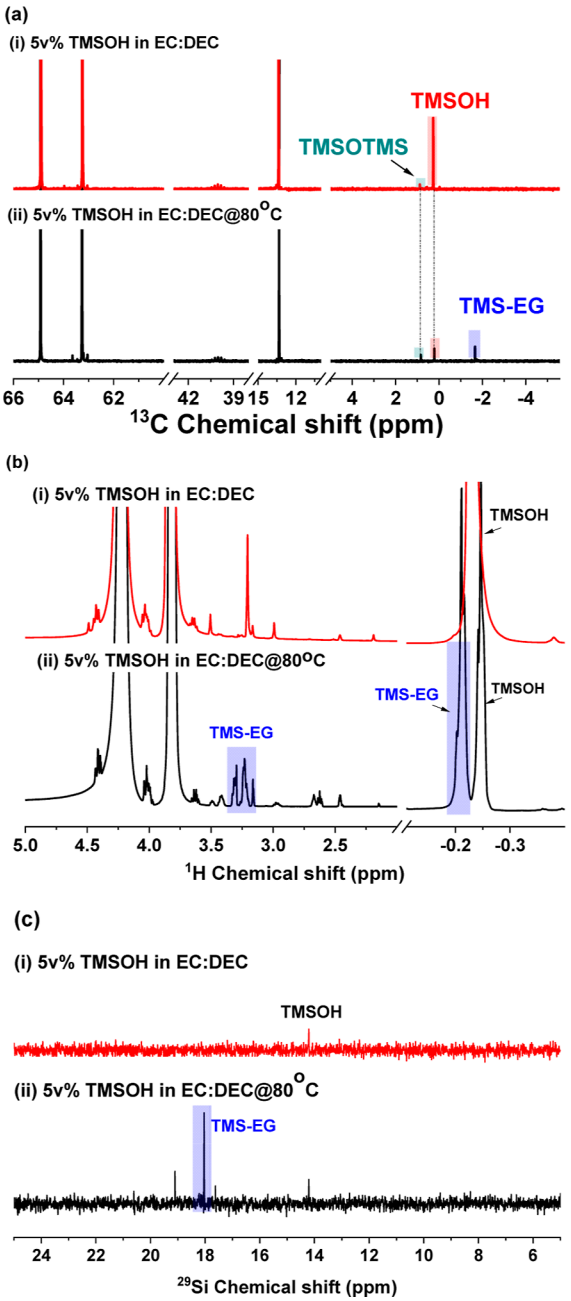

Figure 5. (a) ^{13}C, (b) ^{1}H, and (c) ^{29}Si NMR spectra of 5 vol % TMSOH in EC/DEC mixture at (i) RT and (ii) 80 °C.

TMSOH is identified at 0.25, −0.23, and 14.26 ppm in the ^{13}C, ^{1}H, and ^{29}Si NMR spectra, respectively. It reveals that TMSOH is not involved in any recordable side reactions with the carbonate solvents at RT. TMSOTMS, which is present at the level of impurity, is detected in the mixture at RT in the ^{13}C NMR spectrum as a small signal at 0.86 ppm [Figure 5a(i)]. Its corresponding signal in the ^{1}H NMR spectrum, however, could not be separated from the intense TMSOH signal.

The mixture was then heated to 80 °C and then brought back to RT, after which the NMR spectrum was recorded. The ^{13}C, ^{1}H, and ^{29}Si NMR spectra of the mixture are shown in Figure 5a(ii),b(ii), and c(ii), respectively. The ^{13}C NMR spectrum of the mixture still shows the existence of TMSOTMS; however, the signal for TMSOH decreases, and a new signal appears at −1.64 ppm. This signal at −1.64 ppm is attributed to a TMS derivative with EG (hereafter denoted as TMS-EG), formed as a result of a ring-opening reaction of the surrounding EC molecule triggered by TMSOH (reaction 9). This reaction also leads to the formation of carbondioxide.

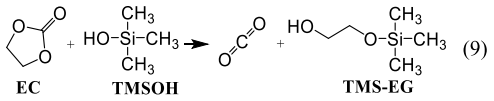

EC ring-opening occurs either by cleavage of the C−O ether bond between the ethylene and carbonate units, followed by the separation of the C−O ether bond between the carbonate C and ether O (pathway 1 in Scheme 1) unit, or by cleavage of the C−O bond between the carbonate C and ether O, followed by separation of the C−O bond between the carbonate and ethylene unit (pathway 2 in Scheme 1). In either case, the resulting products are the same.

In the ^{1}H NMR spectrum as shown in Figure 5b(ii), the peak at −0.23 ppm is attributed to the TMS group of TMS-EG, whereas the group of peaks centered around 3.3 ppm is attributed to the alkyl chain protons of the TMS-EG compound.

The ^{29}Si NMR spectrum of the mixture at RT shows the existence of the TMSOH signal at 14.26 ppm. In the heated sample, in addition to TMSOH, two new signals appear at 18.01 and 19.08 ppm. The intense signal at 18.01 ppm is attributed to TMS-EG. The low amount of TMSOTMS is not detected under ^{29}Si NMR due to its low sensitivity. The signal at 19.08 ppm could not be exactly identified but is believed to be a contribution from the species formed as a result of the further polymerization reaction of the surrounding EC solvent molecule induced by the TMS-EG, so formed (reaction 10).

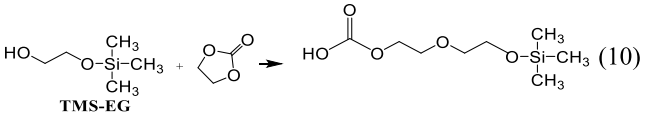

The ring-opened EC with retained carbonate is likely to form as a result, contributing to the signal at 19.08 ppm.

To further corroborate our results, GC−MS on the same samples was performed, and the results are presented in Figure 6. For comparison, the chromatogram of baseline EC/DEC is presented in Figure 6a. In addition to the EC and DEC as the main contents (at 5.79 and 2.74 min, respectively), Figure 6b,c demonstrates the chromatogram of the TMSOH in EC/DEC at RT and 80 °C, respectively, where TMSOH is observed as a signal at the retention time of 1.68 min. Indeed, the presence of TMS-EG as the ring-opened reaction product is confirmed for the reaction mixture at elevated temperatures (Figure 6c). It has a peak with the m/z value of 75, 73, 103, and 119 (see Supporting Information S5) observed at the retention time of 2.87 min. Moreover, TMSOTMS was confirmed in both

https://doi.org/10.1021/acs.jpcc.3c07505
J. Phys. Chem. C 2024, 128, 1654−1662

Scheme 1. Scheme Showing the EC Ring-Opening Reaction Pathways Triggered by TMSOH

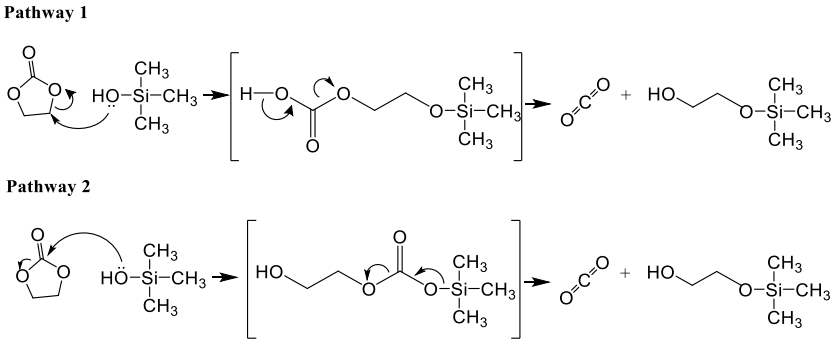

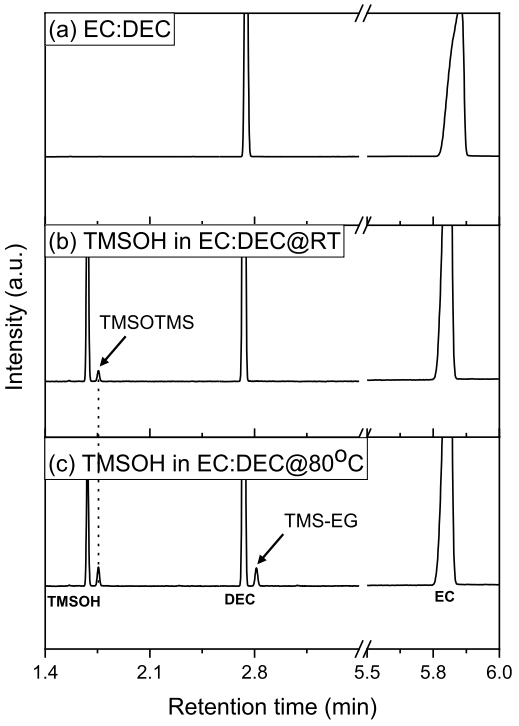

Figure 6. GC−MS spectra of (a) EC/DEC as baseline, (b) 5 vol % TMSOH in EC/DEC at RT, and (c) 5 vol % TMSOH in EC/DEC at 80 °C.

samples. It has a peak with the m/z value of 147 and 73 observed at the retention time of 1.75 min.

Contrary to our previous result where TMSOTMS is found to be the most likely product of the TMSPa and H_2O reaction, TMSOTMS is not found to be the end product here. This rules out that TMSOTMS forms through the TMSOH dimerization reaction (reaction 4) but rather points into the direction that TMSOTMS is the adduct of TMSPa and TMSOH reaction (reaction 5). The result here is also in agreement with the finding that H_2O reacts with EC more favorably than TMSOH does. Thus, it can be concluded that while the formation of TMS-EG at the expense of EC is in principle an unwanted parasitic reaction in a Li-ion cell, it should be noted that this reaction is only substantially activated at elevated temperatures in comparison to EC ring-opening catalyzed by H_2O, which proceeds substantially already at ≥40 °C.[24] Thus, the results underline the advantages of TMSPa as an electrolyte additive in LIBs. TMSPa scavenges the residual H_2O and therefore prevents the EC solvent decomposition and several subsequent harmful side reactions. Moreover, the TMSPa decomposition products are not as reactive toward electrolyte solvents as the water with the virtually stable TMSOTMS as the end product. In this context, it can be pointed out that no observable alteration in the color of the solutions upon the introduction of either water or TMSPa was observed.

CONCLUSIONS

Deeper insights into the reaction pathways of silyl-phosphate-based additives, here exemplified by TMSPa, toward H_2O in LIBs have been presented. Based on the evidence from NMR and GC−MS analysis as well as MD-DFT simulations, a mechanism is proposed.

Si−O bonds within TMSPa react with residual H_2O in the presence of carbonate solvents to form TMSOH and H_3PO_4. TMSOH reacts subsequently with unreacted TMSPa to form the less reactive TMSOTMS dimer. A risk, however, is that the resulting TMSOH performs a nucleophilic attack on and ring-opens EC to form TMS-EG, albeit at a very low rate at RT. The activation energy required to open up the EC ring by TMSOH is much higher than the energy required by the significantly more mobile H_2O. In a practical scenario, it is highly desirable to let TMSPa scavenge H_2O to form less reactive TMS-based compounds. This also hints in the direction that H_2O is a stronger nucleophile than TMSOH. The computational results further suggest that the ability of the reaction products to form energetically favorable intermolecular interactions such as hydrogen bonding is important for the efficient breakage of the O−Si bond of TMSPa.

Our study points to the chemical stability of organosilicon additives in typical LIB electrolyte solutions, which raises questions as to whether the cathode protective agent is the parent compound itself or the polymerized species of the additive molecule. Though these results deserve more detailed investigations as a function of electrochemical cycling and aging conditions of Li-ion cells as well as of synergetic effects in the presence of other additives, the present model study has proven to be relevant and paves the way for further studies dedicated to improve the lifespan of LIBs. We believe that a comprehensive insight combining simple and systematic experimental measurements with first-principles calculations can represent an important breakthrough point.

ASSOCIATED CONTENT

Supporting Information

The Supporting Information is available free of charge at https://pubs.acs.org/doi/10.1021/acs.jpcc.3c07505.

https://doi.org/10.1021/acs.jpcc.3c07505
J. Phys. Chem. C 2024, 128, 1654−1662

Extended ^{1}H, ^{31}P, ^{29}Si NMR spectra, mass spectra from GC−MS, and computational details (PDF)

AUTHOR INFORMATION

Corresponding Authors

Neeha Gogoi − *Department of Chemistry, Ångström Laboratory, Uppsala University, SE-751 21 Uppsala, Sweden;* orcid.org/0000-0002-0481-5544; Email: neeha.gogoi@kemi.uu.se

Erik J. Berg − *Department of Chemistry, Ångström Laboratory, Uppsala University, SE-751 21 Uppsala, Sweden;* orcid.org/0000-0001-5653-0383; Email: erik.berg@kemi.uu.se

Authors

Wandi Wahyudi − *Department of Chemistry, Ångström Laboratory, Uppsala University, SE-751 21 Uppsala, Sweden*

Jonas Mindemark − *Department of Chemistry, Ångström Laboratory, Uppsala University, SE-751 21 Uppsala, Sweden;* orcid.org/0000-0002-9862-7375

Guiomar Hernández − *Department of Chemistry, Ångström Laboratory, Uppsala University, SE-751 21 Uppsala, Sweden;* orcid.org/0000-0002-2004-5869

Peter Broqvist − *Department of Chemistry, Ångström Laboratory, Uppsala University, SE-751 21 Uppsala, Sweden;* orcid.org/0000-0002-9842-4332

Complete contact information is available at: https://pubs.acs.org/10.1021/acs.jpcc.3c07505

Notes

The authors declare no competing financial interest.

ACKNOWLEDGMENTS

The authors acknowledge the Knut and Alice Wallenberg (KAW) Foundation (grant 2017.0204), Swedish Research Council (2016-04069), and Stiftelsen för Strategisk Forskning (SSF, FFL18-0269) for financial support and StandUp for Energy and the national strategic e-Science program eSSENCE for base funding. The simulations were performed on resources provided by the Swedish National Infrastructure for Computing (SNIC) at HPC2N and NSC.

REFERENCES

(1) Barlowz, C. G. Reaction of water with hexafluorophosphates and with Li bis(perfluoroethylsulfonyl)imide salt. *Electrochem. Solid-State Lett.* **1999**, *2*, 362−364.

(2) Sinha, N. N.; Burns, J. C.; Dahn, J. R. Comparative Study of Tris(trimethylsilyl) Phosphate and Tris(trimethylsilyl) Phosphite as Electrolyte Additives for Li-Ion Cells. *J. Electrochem. Soc.* **2014**, *161*, A1084−A1089.

(3) Han, Y. K.; Yoo, J.; Yim, T. Why is tris(trimethylsilyl) phosphite effective as an additive for high-voltage lithium-ion batteries? *J. Mater. Chem. A* **2015**, *3*, 10900−10909.

(4) Peebles, C.; Sahore, R.; Gilbert, J. A.; Garcia, J. C.; Tornheim, A.; Bareño, J.; Iddir, H.; Liao, C.; Abraham, D. P. Tris(trimethylsilyl) Phosphite (TMSPi) and Triethyl Phosphite (TEPi) as Electrolyte Additives for Lithium Ion Batteries: Mechanistic Insights into Differences during LiNi 0.5 Mn 0.3 Co 0.2 O 2 -Graphite Full Cell Cycling. *J. Electrochem. Soc.* **2017**, *164*, A1579−A1586.

(5) Mai, S.; Xu, M.; Liao, X.; Hu, J.; Lin, H.; Xing, L.; Liao, Y.; Li, X.; Li, W. Tris(trimethylsilyl)phosphite as electrolyte additive for high voltage layered lithium nickel cobalt manganese oxide cathode of lithium ion battery. *Electrochim. Acta* **2014**, *147*, 565−571.

(6) Park, M. W.; Park, S.; Choi, N. S. Unanticipated Mechanism of the Trimethylsilyl Motif in Electrolyte Additives on Nickel-Rich Cathodes in Lithium-Ion Batteries. *ACS Appl. Mater. Interfaces* **2020**, *12*, 43694−43704.

(7) Guéguen, A.; Bolli, C.; Mendez, M. A.; Berg, E. J. Elucidating the Reactivity of Tris(trimethylsilyl)phosphite and Tris(trimethylsilyl)-phosphate Additives in Carbonate Electrolytes - A Comparative Online Electrochemical Mass Spectrometry Study. *ACS Appl. Energy Mater.* **2020**, *3*, 290−299.

(8) Bolli, C.; Guéguen, A.; Mendez, M. A.; Berg, E. J. Operando Monitoring of F - Formation in Lithium Ion Batteries. *Chem. Mater.* **2019**, *31*, 1258−1267.

(9) Gogoi, N.; Bowall, E.; Lundström, R.; Mozhzhukhina, N.; Hernández, G.; Broqvist, P.; Berg, E. J. Silyl-Functionalized Electrolyte Additives and Their Reactivity toward Lewis Bases in Li-Ion Cells. *Chem. Mater.* **2022**, *34*, 3831−3838.

(10) Frisch, M. J.; Trucks, G. W.; Schlegel, H. B.; Scuseria, G. E.; Robb, M. A.; Cheeseman, J. R.; Scalmani, G.; Barone, V.; Mennucci, B.; Petersson, G. A.; Nakatsuji, H.; Caricato, M.; Li, X.; Hratchian, H. P.; Izmaylov, A. F.; Bloino, J.; Zheng, G.; Sonnenberg, J. L.; Had, M. *Gaussian 09*; Gaussian, Inc.: Wallingford CT, 2016.

(11) Becke, A. D. Density-functional thermochemistry. III. The role of exact exchange. *J. Chem. Phys.* **1993**, *98*, 5648−5652.

(12) Lecklider, T. Development of the Colic-Salvetti correlation-energy into a functional of the electron density formula. *Eval. Eng.* **2011**, *50*, 36−39.

(13) Vosko, S. H.; Wilk, L.; Nusair, M. Accurate spin-dependent electron liquid correlation energies for local spin density calculations: a critical analysis. *Can. J. Phys.* **1980**, *58*, 1200−1211.

(14) Stephens, P. J.; Devlin, F. J.; Chabalowski, C. F.; Frisch, M. J. Ab Initio Calculation of Vibrational Absorption and Circular Dichroism Spectra Using Density Functional Force Fields. *J. Phys. Chem.* **1994**, *98*, 11623−11627.

(15) Grimme, S.; Antony, J.; Ehrlich, S.; Krieg, H. A consistent and accurate ab initio parametrization of density functional dispersion correction (DFT-D) for the 94 elements H-Pu. *J. Chem. Phys.* **2010**, *132*, 154104.

(16) Shao, Y.; Hellström, M.; Mitev, P. D.; Knijff, L.; Zhang, C. PiNN: A Python Library for Building Atomic Neural Networks of Molecules and Materials. *J. Chem. Inf. Model.* **2020**, *60*, 1184−1193.

(17) Bannwarth, C.; Caldeweyher, E.; Ehlert, S.; Hansen, A.; Pracht, P.; Seibert, J.; Spicher, S.; Grimme, S. Extended tight-binding quantum chemistry methods. *Wiley Interdiscip. Rev. Comput. Mol. Sci.* **2021**, *11*, 1−49.

(18) Bannwarth, C.; Ehlert, S.; Grimme, S. GFN2-xTB - An Accurate and Broadly Parametrized Self-Consistent Tight-Binding Quantum Chemical Method with Multipole Electrostatics and Density-Dependent Dispersion Contributions. *J. Chem. Theory Comput.* **2019**, *15*, 1652−1671.

(19) Shao, Y. *Simulating Ion Transport in Electrolyte Materials with Physics-Based and Machine-Learning Models*; Uppsala University, 2022.

(20) Hjorth Larsen, A.; Jørgen Mortensen, J.; Blomqvist, J.; Castelli, I. E.; Christensen, R.; Dułak, M.; Friis, J.; Groves, M. N.; Hammer, B.; Hargus, C.; et al. The atomic simulation environment - A Python library for working with atoms. *J. Phys.: Condens. Matter* **2017**, *29*, 273002.

(21) Allouche, A. Packmol: A Package for Building Initial Configurations for Molecular Dynamics Simulations. *J. Comput. Chem.* **2011**, *32*, 174−182.

(22) Yim, T.; Woo, S. G.; Lim, S. H.; Cho, W.; Song, J. H.; Han, Y. K.; Kim, Y. 5V-class high-voltage batteries with over-lithiated oxide and a multi-functional additive. *J. Mater. Chem. A* **2015**, *3*, 6157−6167.

(23) Qi, X.; Tao, L.; Hahn, H.; Schultz, C.; Gallus, D. R.; Cao, X.; Nowak, S.; Röser, S.; Li, J.; Cekic-Laskovic, I.; et al. Lifetime limit of tris(trimethylsilyl) phosphite as electrolyte additive for high voltage lithium ion batteries. *RSC Adv.* **2016**, *6*, 38342−38349.

(24) Metzger, M.; Strehle, B.; Solchenbach, S.; Gasteiger, H. A. Hydrolysis of Ethylene Carbonate with Water and Hydroxide under

Battery Operating Conditions. *J. Electrochem. Soc.* **2016**, *163*, A1219−A1225.

https://doi.org/10.1021/acs.jpcc.3c07505
J. Phys. Chem. C 2024, 128, 1654−1662